Preprints of the 21st IFAC World Congress (Virtual)
Berlin, Germany, July 12-17, 2020

Modeling and Temperature Control of Retinal Laser Therapy ⋆

Hossam S. Abbas [*,**] **Christopher Kren** [**] **Veit Danicke** [**]
Dirk Theisen-Kunde [**] **Ralf Brinkmann** [**,***]

[*] *Institute for Electrical Engineering in Medicine, University of Lübeck, Lübeck, Germany (e-mail: h.abbas@uni-luebeck.de).*
[**] *Medical Laser Center Lübeck, Lübeck, Germany.*
[***] *Institute of Biomedical Optics, University of Lübeck, Lübeck, Germany.*

Abstract: The development of a noninvasive technique to measure tissue temperature during retinal laser treatment allows feedback control approaches to regulate the temperature rise to desired values. The main challenge is to provide fast and consistent good control performance regardless the uncertainty of the dynamics of the temperature increase at the different irradiated spots on the retina, which is due to the large variance of the retinal light absorption. In this paper, we demonstrate a successful experimental application in ex-vivo of robust $\mathcal{H}_\infty$ PID control to handle such a control problem. The system input is the applied laser power and its output is the temperature increase. Based on measurements of input-output data, we employ system identification to model the range of the system dynamics at different retinal irradiation sites. Then, we use a loop shaping approach to express the performance specifications of the closed-loop system and we synthesize accordingly the controller using efficient robust $\mathcal{H}_\infty$ synthesis tools for fixed structure controllers. The experimental implementation of the closed-loop system for tracking different reference temperatures demonstrates the achievement of the control objectives consistently at the different irradiation sites.

Keywords: Biomedical control systems, System identification, $\mathcal{H}_\infty$-robust control, PID control.

1. INTRODUCTION

Laser irradiation is a standard transpupillary therapy for several retinal diseases such as diabetic retinopathy. The treatment operation depends on choosing an appropriate laser power of a *continuous wave laser* (cw-laser) device to heat up the irradiated site on the retina until desired heating effects appear, like a visible lesion. The heating effects due to the temperature rise depend on the light absorption properties of the irradiated sites. The current treatment depends on visible inspection of the irradiation sites of previous lesions owing to the typically short irradiation time around 0.1 s. Thus, ophthalmologists can adjust manually the required amount of laser power for the following spots. However, due the strong in-homogeneity of the thermal absorption rates of the irradiated sites on the retina, it is very difficult to achieve uniform heating effects using such manual titration, which can lead to over/under treatment effects, pain, bleeding, visual field defects and other complications, see, e.g., Mainster (1999).

The recent development of an *optoacoustic* (OA) method by Brinkmann et al. (2012) to measure noninvasively temperature increase at the retinal irradiation sites during the treatment allows the application of feedback control to regulate automatically the temperature increase to a desired value. Temperature feedback-controlled laser treatment can automatically modify the laser power to proper values, which can lead to uniform thermal effects. Several approaches have been introduced for controlling the temperature rise using the OA temperature measurement; however, most of them such as the approaches of Schlott et al. (2012) and Baade et al. (2017), were based on empirical open-loop control. The first trail of using proper automatic control engineering was introduced in Herzog et al. (2018) based on $\mathcal{H}_\infty$ control; it proposed a robust closed-loop control, which can achieve consistently about 50 ± 6 ms irradiation time to track a desired temperature value. However, safety limits regarding the applied laser power were not taken in account by the closed-loop system which makes it prone to saturation effects and possible termination due excessive use of laser power. Moreover, it is usually desired to provide fast irradiation time of about 40 ms or less to follow a desired temperature.

The large variance of the absorption rates at the retinal irradiation sites demands robust control strategies to deal with the uncertainty of the corresponding rates of the temperature increase and to achieve consistent temperature rise regardless the heterogeneity of the absorption. Moreover, the controller should also respect safety limits of the applied laser power and attenuate disturbances/noise effects. $\mathcal{H}_\infty$ control approach offers very efficient methods, see, e.g., Zhou and Doyle (1998), Skogestad and Postleth-

⋆ This work is supported by the German Ministry of Research and Technology, BMBF, grant No. 13GW0043, alliance I-cube. The first author is currently funded by the Deutsche Forschungsgemeinschaft (DFG, German Research Foundation) — Project No. 419290163.

waite (2005), supported by software tools, such as that of Balas et al. (2011), to systematically achieve performance shaping of the control system. It can also provide robust stability and performance guarantees.

In order to design the required controller, we adopt in this paper $\mathcal{H}_\infty$ control using mixed sensitivity loop shaping, see, e.g., Skogestad and Postlethwaite (2005), which can easily translate the required control objectives in the design. However, for such a model based control approach, a mathematical model is required to describe the relation between the laser power and the temperature increase at different irradiation sites. For this purpose, we use system identification, Ljung (1999), based on measured data sets. For practical implementation, we design a robust PID controller using recently devloped techniques for designing robust fixed-structure $\mathcal{H}_\infty$ controllers of Apkarian et al. (2015). The implementation of the PID controller includes an integral sum correction algorithm to provide simple anti-windup to deal with laser power limits. The experimental results in ex-vivo of the proposed controller show fast and consistent response for tracking desired temperature values within irradiation time of 32 ± 7 ms.

The paper is organized as follows: Section 2 illustrates the OA measurement system, the experimental setup and the model of the system. The control design approach is detailed in Section 3. The simulation and experimental results are demonstrated and discussed in Section 4. Finally, the conclusion is drawn in Section 5.

2. MODELING

A successful feedback control system for controlling the retinal temperature increase relies essentially on the availability of a mathematical model, which can describe the dynamical relation between the temperature increase $\Delta T(t)$ and the applied lased power P_{L} at different retinal irradiation sites. In this section, we first discuss briefly the OA method of Brinkmann et al. (2012) for measuring the temperature at the irradiated sites, then an overview of the experimental setup used in this work is given. Finally, we present the system identification approach we used to develop a dynamical model for the system.

2.1 OA Temperature Measurement

The principle of the OA temperature measurement is to emit laser pulses on the retina, which excites the irradiated tissue to generate bipolar pressure waves (ultrasonic waves) propagating through the eye globe. Such waves can then be detected by an ultrasonic transducer embedded in a contact lens. The peak amplitude of the pressure wave is proportional to the temperature at the irradiated site via the so-called Grüneisen coeffiecient, which is used to compute the corresponding temperature given the peak pressure measurement. The OA temperature measurement has been verified experimentally in Brinkmann et al. (2012) with direct temperature measurements using thermocouples and clinical trials.

2.2 Experimental Setup

The experimental setup considered in this work is located at the Medical Laser Center Lübeck (MLL), Lübeck, Germany, a simplified schematic diagram is shown in Fig. 1. It consists of two laser devices: The heating (treatment) cw-laser, which is a frequency doubled Nd:YAG (Visulas 532 s, Carl Zeiss Meditec AG, wave length $\lambda = 532$ nm, continuous wave) and the measurement laser, which is a frequency doubled Q-switched Nd:YLF (QC-523-1000, CrystaLaser, $\lambda = 523$ nm, pulse width 75 ns, $f = 3$ kHz) generating one pulse every 1/3 ms. The heating laser basically implements the laser power computed by the controller, whereas, the measurement laser is used to generate the laser pulses into the radiation sites for measuring the temperature as discussed in Section 2.1. The radiations from both lasers are coupled via a microscope objective into a multimode fiber and focused onto the retina for the irradiation. A piezo ceramic ultrasonic transducer with high sensitivity and resonance frequency of 1 MHz embedded in a contact lens is used to detect the produced pressure waves. The signal processing and the control algorithm calculations are performed using a PC running LabView, see Baade et al. (2017) for more details. In this work, we consider experiments on ex vivo explants from porcine eyes [1] at room temperature $T_{\mathrm{room}} = 20^{\mathrm{o}}$C.

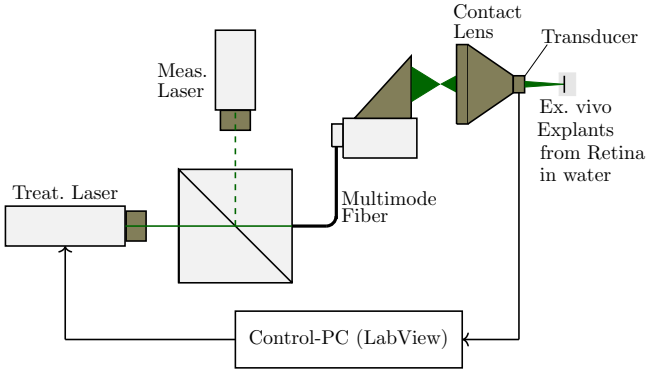

Fig. 1. Experimental Setup: A standard treatment laser is combined with a probe (measurement) laser. Both are transmitted via a quartz fiber to a standard slit-lamp. A piezo-transducer is embedded in a contact lens (Mainster OMRA-S laser Lens) used to measure the OA signal, and hence, the temperature value.

2.3 System Identification

System identification, see Ljung (1999), is an engineering tool for creating mathematical models of dynamical systems from experimental measured data. In this work, we consider discrete-time linear time-invariant (LTI) models with transfer function representation as follows:

$$\frac{y(k)}{u(k)} = q^{-n_{\mathrm{k}}} \frac{b_0 + b_1 q^{-1} + \cdots + b_{n_{\mathrm{b}}} q^{-n_{\mathrm{b}}}}{1 + a_1 q^{-1} + \cdots + a_{n_{\mathrm{a}}} q^{-n_{\mathrm{a}}}}, \qquad (1)$$

where $u(k)$ and $y(k)$ are the input and output of the system, respectively, at a sampling time instant k, q^{-1} is the backward shift operator, i.e., $q^{-1}u(k) = u(k-1)$, $b_0, b_1, \cdots, a_1, \cdots$ are constant coefficients for parameterizing the system, n_{a} is the model order such that $(n_{\mathrm{a}} \geq n_{\mathrm{b}})$ and n_{k} represents time delay. In system identification, given the values of $n_{\mathrm{a}}, n_{\mathrm{b}}, n_{\mathrm{k}}$, the constant coefficients are determined using measured input-output data of the system. In most of systems, the measured output is usually

[1] Retina tissue are taken from pig eyes and used within 6 hours.

affected by disturbance/noise v. In order to characterize the properties of v, thus, better describing the measured output, model structures are used in system identification. These include AutoRegressive with eXternal input (ARX), Output-Error (OE), AutoRegressive moving Average with eXternal input (ARMAX), and Box-Jenkins (BJ) models. They are different in the way that v is described via a so-called noise model with white noise input e, see Fig. 2. The model structures range from the simplest structure

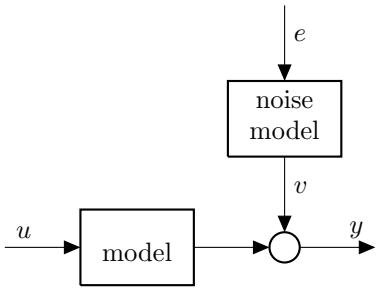

Fig. 2. Model structure with model noise characterization.

(the ARX) to the complicated one (the BJ), which can provide the most linear rigorous noise model for describing v. Commonly, the prediction error minimization approach is used to obtain the constant coefficients of the transfer function model, in which the error between the measured output y and the simulated output $\hat{y}$ of the identified model is minimized over the coefficients of the system model and the noise model.

For the system under study here, the input is the laser power P_{L} and the output is the temperature increase ΔT. Based on 528 input-output data sets of (P_{L}, ΔT), see Fig. 3, from different pig eyes, it turns output that the relationship between ΔT and P_{L} can be described by the first-order differential equation, Herzog et al. (2018),

$$\tau \Delta \dot{T}(t) = -\Delta T(t) + \kappa P_{\mathrm{L}}(t), \tag{2}$$

where τ, κ are the time constant and the static gain, respectively, of the model. The model (2) indicates that $n_{\mathrm{a}} = n_{\mathrm{b}} = n_{\mathrm{k}} = 1$ in (1), thus, three coefficients b_0, b_1, a_1 can be considered to parameterize a transfer function model for the system. In principle, these coefficients characterize τ and κ of the system. Due to the heterogeneity of the retinal absorption rate, the coefficients b_0, b_1, a_1 are dependent on the irradiation site absorption properties, which are related to its amount of pigmentation and its thickness. In order to design an appropriate robust controller, it is very important to identify the range of values of b_0, b_1, a_1 (and consequently of τ and κ). Therefore, different data sets, in total 528 input-output date sets, have been gathered from different sites on the retina of several pig eyes. The experiments for collecting the data have been carried out by applying different two level steps input over three phases as shown in Fig. 3. Note that in the first 10 ms only laser pulses are applied, i.e., $P_{\mathrm{L}} = 0$, this is a necessary phase of each experiment for calibrating the temperature measurement according to the irradiation site property, see Baade et al. (2017) for more details. In the second and third phases (20 ms for each) the two different levels of P_{L} are applied while the temperature rise is recorded.

Next, the system identification is performed for each data set, where four models have been identified with the

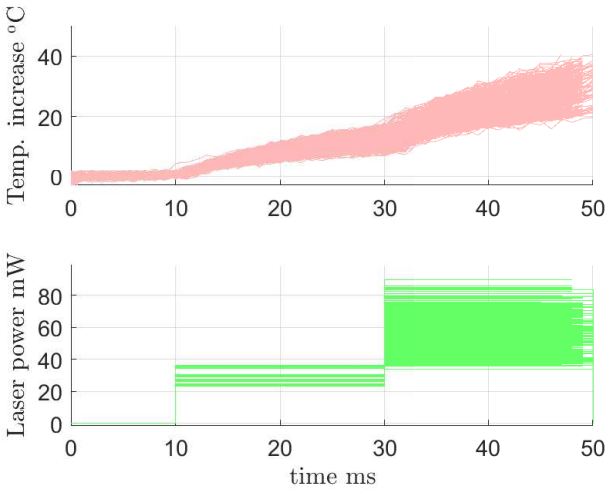

Fig. 3. Superimposed plots of the input and output measurements for system identification.

different structures as discussed above. The identification problem has been solved using the system identification toolbox in Matlab, Ljung (2018). Each model is validated using the best fit rate (BFR) criterion given by

$$\mathrm{BFR} = \max\left(0, \frac{\|y - \hat{y}\|_2}{\|y - \bar{y}\|_2}\right) \cdot 100 \ \ \% \tag{3}$$

where $\|\cdot\|_2$ indicates a vector 2-norm, $\bar{y}$ represents the mean value of the measured output y. The BFR evaluates the error between the measured and simulated data in %. For each data set, we checked the model structure whose BFR is the highest among the others. We observed that the BJ model structure gave the best BFR for most of data sets, therefore, we select all models as BJ models for compatibility. Then, the time constant and static gain of each model have been calculated from the identified coefficients. Table 1 shows the minimum, maximum, mean and standard deviation (std) of the BFR, τ and κ of the identified models. The identified 528 models demonstrate

Table 1. Results of the identified model.

	[min, max]	mean±std
BFR %	[84.19, 95.65]	91.76 ± 1.91
τ ms	[7.27, 77.65]	23.94 ± 13.81
κ $^{\mathrm{o}}\mathrm{CmW}^{-1}$	[0.33, 1.86]	0.77 ± 0.24

proportionate BFR as shown in the table. The time constant and static gain as shown in Table 1 assess the physical proprieties of the models, and their values provide realistic ranges from the physiological point of view and confirm their ranges of uncertainties to be used in control design. To visualize the quality of the models, Fig. 4 shows validation plots for the best and worst models according to the BFR values, it indicates that the models have captured well the dynamics of the temrpature rise at the different irradiation sites.

It is worth to mention that the models used in Herzog et al. (2018) had been identified from the same data used here; nevertheless, the identitifcation method used in Herzog et al. (2018) had been carried out by writing the prediction error in linear regression form, thus, ignored the noise/disturbance in the data, to solve the identification problem as a linear least squares (LS) problem. However,

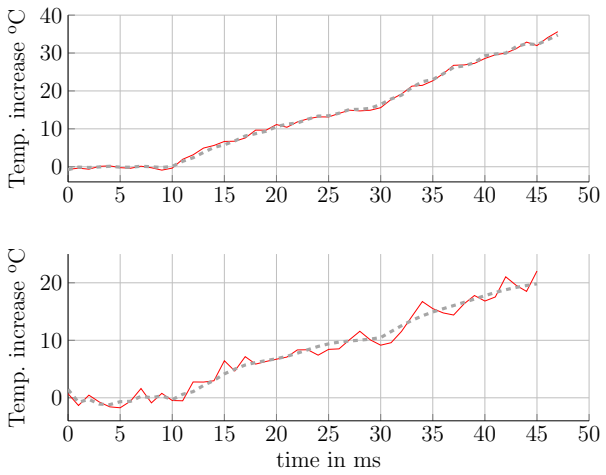

Fig. 4. Validation plots with BFR of 95.65% (up) and 84.19% (down): measured data in red-solid and simulated data in gray-dashed.

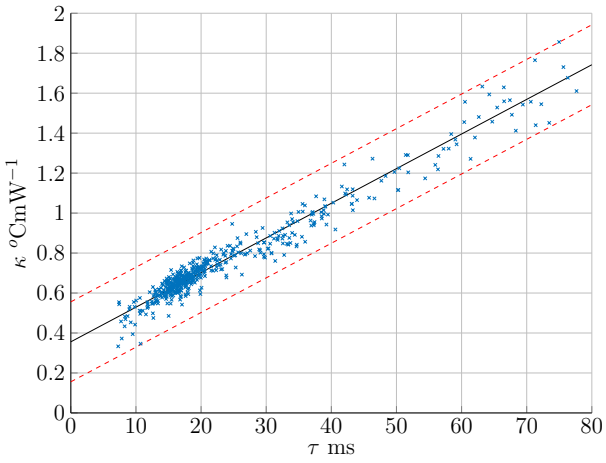

Fig. 5. The linear correlation between the time constants and the static gains of the identified models.

LS leads to biased parameters estimation — except for ARX model structure — when it is applied on noisy data as the case here, see Ljung (1999). This had resulted in wider ranges for τ and κ than those obtained here, which can lead to more conservative controllers.

Finally, it turns out like the case in Herzog et al. (2018), a linear correlation between τ and κ as shown in Fig. 5, which can be given by

$$\kappa = 17.33\tau + 0.36 \pm 0.2. \tag{4}$$

This is exploited in the control design as shown below.

3. ROBUST $\mathcal{H}_\infty$ PID CONTROLLER DESIGN

In this section, we demonstrate the control objectives and the design procedure adopted for controlling the temperature rise at the retinal irradiation site based on the model obtained in the previous section. We consider $\mathcal{H}_\infty$-norm optimal control to optimally design the parameters of the proposed PID controller.

The $\mathcal{H}_\infty$-norm of a transfer function model measures its maximum gain over all frequencies. It can be used to specify performance for a feedback interconnection in terms of a generalized plant P, thus, the interconnection includes a controller K, which can be synthesized to stabilizes the closed-loop interconnection and achieves a performance index γ that provides an upper bound on the $\mathcal{H}_\infty$-norm of the closed-loop system. The uncertainty (Δ) of the model can be included as well via *linear fraction representation* (LFR) of P and the uncertainty, as shown in Fig. 6, and hence, robust controllers can be design, which can provide robustness against the range of uncertainty in the model, i.e., for all $\Delta \in \mathbf{\Delta}$, where $\mathbf{\Delta}$ represents the set of all admissible values of the uncertainty Δ. Currently, efficient software tools are readily available, e.g., in the Matlab Robust Control Toolbox, Balas et al. (2011), for $\mathcal{H}_\infty$ design. The proposed generalized plant interconnection, i.e., P, translates the performance specifications into the objective of minimizing a closed-loop $\mathcal{H}_\infty$-norm. The problem of designing a robust $\mathcal{H}_\infty$ controller is an optimization problem given as follows

$$\gamma = \min_K \|T_{\mathrm{zw}}^{\infty}\|_\infty, \quad \forall \Delta \in \mathbf{\Delta}, \tag{5}$$

where T_{zw}^{∞} is the closed-loop transfer function between w and z, which define the performance channels, see Fig. 6. In this work, we deal with parametric uncertainty and we want to design PID controllers, i.e., strucutred controllers, with robust stability and performance guarantees. Recently, methods have been introduced, e.g., in Apkarian et al. (2015), to design $\mathcal{H}_\infty$ control with fixed structured controllers as well as robust stability and performance guarantees; however, the challenging part of the design is to provide meaningful performance specifications.

The design objectives considered for the system under study is basically to provide responsibly fast tracking of the reference (aim) temperature to approach its value within less than 40 ms without overshoot, oscillations or steady state errors and with a laser power less than $P_{\mathrm{Llim}} = 120$ mW. A mixed sensitivity loop-shaping approach is adopted to achieve the control objectives. We carry out the design directly in discrete time with a sampling time of 1 ms to avoid performance deterioration due to sampling. The generalized plant shown in Fig. 7 is used to express the design specifications on the control system. The performance channels are $w = [r \;\; d]^\top$, where r and d, denote reference and disturbance inputs, respectively, and $z = [z_{\mathrm{K}} \;\; z_{\mathrm{S}}]^\top$ is a fictitious output vector to express design specifications. The model with uncertainty developed in the previous section is represented in LFR form by the interconnection between the block G, which indicates the nominal model, and the uncertainty Δ block. The relation between the uncertain parameters τ and κ as in (4) has been exploited to reduce the size of the Δ block, $\Delta \in \mathbb{R}^3$. The design specifications are expressed via the weighting filters W_{S} and W_{K} to shape the sensitivity S and the control sensitivity KS functions, respectively, for the feedback system and W_{R} is a filter used to shape the reference input. Including W_{R} in the closed-loop implementation can have a considerable effect on improving the reference tracking. Using the discrete-time integrator and derivative blocks in the generalized plant renders the PID parameters, i.e., its proportional gain K_{p}, integral time T_{i}, and derivative time T_{d}, directly the decision variables of the control optimization problem. To achieve the control objectives above W_{S}, W_{K} and W_{R} have been chosen as follows

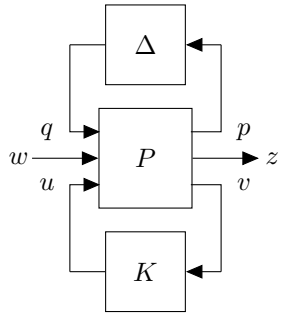

Fig. 6. Interconnection of LFR generalized plant with a robust controller.

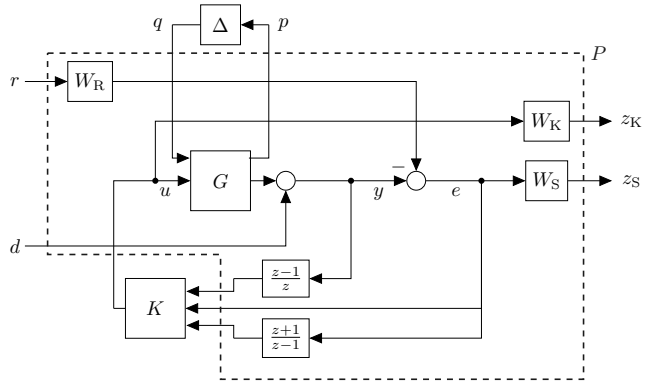

Fig. 7. Detailed generalized plant with shaping filters.

$$W_S = \frac{0.0975z + 0.0775}{z - 0.9998}, \quad W_K = \frac{2.6224z - 2.0364}{z + 0.9534},$$
$$W_R = \frac{0.0089z + 0.0083}{z^2 - 1.7770z + 0.7943}.$$

The optimization problem (5) associated with the generalized plant shown in Fig. 7 has been solved using the Matlab command `systune`, then, the $\mathcal{H}_\infty$ PID controller has been determined with the parameters $K_\mathrm{p} = 2.0673$, $T_\mathrm{i} = 9.1690 \times 10^{-5}$ min, $T_\mathrm{d} = -8.3629 \times 10^{-6}$ min.

To deal with the windup effect of the controller when the limits of the control output, i.e., the laser power, is reached, we use an integral sum correction algorithm. It is implemented online and it works as follows: If $|u_\mathrm{p}(k) + u_\mathrm{i}(k)| > P_\mathrm{limit}$, where u_p, u_i are the control inputs related to the proportional and the integral parts, respectively, then let $u_\mathrm{i}(k) > P_\mathrm{limit} + u_\mathrm{p}(k)$. Note that the derivative actions has not been taken into account. Such algorithm can provide a satisfactory ant-windup action, yet with a very simple implementation. However, more elaborated ant-windup approaches will be considered in the future.

4. EXPERIMNTAL AND SIMULATION RESULTS

The closed-loop experiments have been conducted on different irradiation sites of four different ex vivo explants from porcine eyes at $T_\mathrm{room} = 20^\mathrm{o}$C. In total 122 successful experiments have been performed for tracking aim temperatures $T_\mathrm{aim} = 30, 35, 40, 45, 50^\mathrm{o}$C, where in each experiment a single aim temperature should be tracked. Let the controlled temperature be denoted as $T = \Delta T + T_\mathrm{room}$, $T_\mathrm{room} = 20^\mathrm{o}$C; the OA measurement system measures T with a rate of 3 kHz, however, the controller sampling rate is 1 KHz, due to hardware restrictions [2], therefore, the controller receives the average of three temperature values. To evaluate the closed-loop system performance, we consider the following parameters:

- Rise time, t_rise, which is defined here as the time for T to reach its reference value starting from the room temperature value.
- Max. overshoot, $M = (\max(T) - T_\mathrm{aim})/T_\mathrm{aim} \cdot 100\%$.
- T_ratio, which is the percentage ratio between the average value of T for $t > t_\mathrm{rise}$ and T_aim, which is used to indicate over-/under-heating conditions and to evaluate average steady state errors.

The overshoot values computed by the standard way as above might be greater than its actual value as the value of $\max(T)$ might be enlarged due to inaccuracies of the OA measurement system. Therefore, we include another way to evaluate max. overshoots, which is based on fitting the measured values of T in one experiment by a polynomial, where, 7^th-order polynomials provided acceptable fit. The overshoot in this way is considered as a fourth parameter for evaluating the system performance:

- $M_\mathrm{fit} = (\max(T_\mathrm{fit}) - T_\mathrm{aim})/T_\mathrm{aim} \cdot 100\%$.

We summarize in Table 2 the closed-loop results based on the mean value and the standard deviation of the parameters discussed above for all experiments at all considered aim temperatures. Generally, the tracking performance

Table 2. Summary of experimental Results in terms of mean and standard deviation.

t_rise [ms]	T_ratio [%]	M [%]	M_fit[%]
mean ± std	mean ± std	mean ± std	mean ± std
31.82 ± 6.71	102.17 ± 0.90	9.41 ± 2.69	5.32 ± 1.88

of all aim temperatures at the different irradiation sits is consistent, which is a good indication of the robust performance of the closed loop system with the designed controller. It is demonstrated that all aim temperatures have been reached quite fast within less than 40 ms as demanded. The mean value of T_ratio in Table 2 indicates a consistent small over-treatment condition of 2% in all experiments, which is acceptable. The max. overshoot is relatively high; however, as we mentioned above this could be due to inaccuracies of the value of $\max(T)$, therefore, we assess the max. overshoot based on M_fit, which is reasonable with such fast controller.

Figure 8 shows representative results of the experiments of tracking aim temperatures of $(30, 40, 50)^\mathrm{o}$C in closed-loop and the corresponding laser powers computed by the designed robust PID controller. Note that the closed-loop is switched on after 3 ms, whereas the first 3 ms are used for calibrating the temperature measurement. The tracking performance is very satisfactory for all reference temperatures with smooth control actions. For comparison with the simulation, we have tested the model in closed-loop with values of τ and κ that most likely can produce similar experimental results as depicted in Fig. 8 for both

[2] The laser power computed by the controller is actuated via an acoustic-optic modulator (AOM); the bandwidth of the amplifiers used in the setup to operate the AOM is limited to 1 kHz. Therefore, using 1 kHz sampling rate avoids including the dynamics of these amplifiers in the control design.

the input and the output. These values are $\tau = 22, 20, 15$ ms and $\kappa = 0.837, 0.553, 0.416$ for the tracking simulation of the reference temperatures $(30, 40, 50)$°C, respectively. Such comparison confirms the quality of the identified model we used for designing the controller.

Due to the uncertainty of τ and κ, it has been observed that for some experiments the required P_{L} for tracking the same aim temperature was less or more than those shown in Fig. 8. Note that the experiments have been implemented at different retinal irradiation sites of different pigs' eyes, which might vary significantly in the thermal absorption properties. This has been confirmed in simulation as well. Furthermore, for 7 experiments related to tracking $T_{\mathrm{aim}} = 50$°C, the limit P_{Llim} was active as depicted in Fig. 9; however, due to the ant-wind up algorithm that took just few milliseconds without significant effects on the general response. We extend the time scale in Fig. 9 to show the steady-sate value of P_{L}.

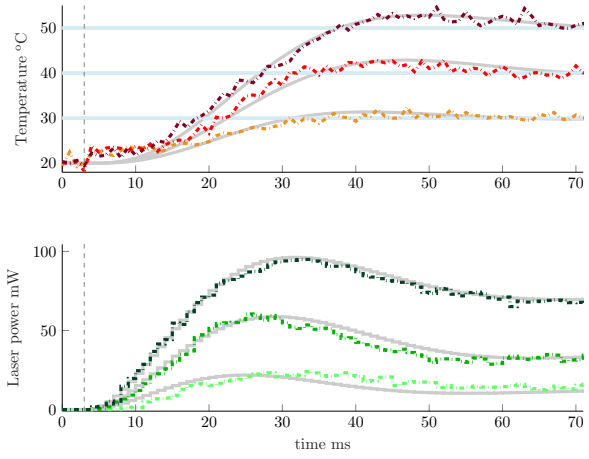

Fig. 8. Comparison between representative experimental and simulation results: $T_{\mathrm{aim}} = 30$°C in orange, 40°C in red and 50°C in burgundy, and the related P_{L} in light-green, green and dark-green, respectively, all the corresponding simulation results in gray.

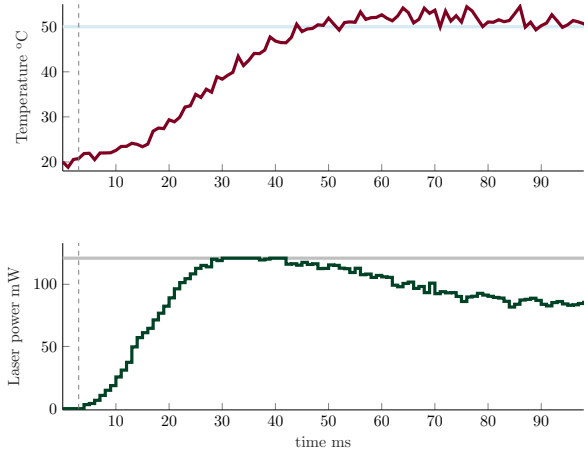

Fig. 9. Experimental results where the laser power limit was active.

5. CONCLUSION

This paper has demonstrated a successful application of automatic control engineering in ex-vivo temperature-controlled retinal laser therapy. The system identification modeling approach has been utilized based on measured input-output data sets to identity a mathematical model with parametric uncertainties, which can describe the dynamical relation between the applied laser power and the temperature rise at the different irradiated tissues. Then, efficient $\mathcal{H}_\infty$ robust control tools have been used for synthesizing a PID control based on the identified model. The proposed robust PID control has achieved reasonably well a uniform temperature rise at different irradiation sites during the retinal laser application. The temperatures within the range $(30 - 50)$°C were attained quite fast within about 32 ± 7 ms of the irradiation duration with an acceptable small over-heating. The control system has the ability to respect safety limits regarding the laser power. The proposed automatic control engineering strategy will have important impact for achieving a balanced and safe retinal laser treatment with minimum intervention from ophthalmologists. Moreover, the approach can be extended to several other hyperthermial stimulation treatments.

REFERENCES

Apkarian, P., Dao, M.N., and Noll, D. (2015). Parametric robust structured control design. *IEEE Transactions on Automatic Control*, 60(7), 1857–1869.

Baade, A., von der Burchard, C., Lawin, M., Koinzer, S., Schmarbeck, B., Schlott, K., Miura, Y., Roider, J., Birngruber, R., and Brinkmann, R. (2017). Power-controlled temperature guided retinal laser therapy. *Journal of Biomedical Optics*, 22(11), 118001–1–11.

Balas, G., Chiang, R., Packard, A., and Safonov, M. (2011). *Robust Control Toolbox for Use with Matlab*.

Brinkmann, R., Koinzer, S., Schlott, K., Ptaszynski, L., Bever, M., Baade, A., Luft, S., Miura, Y., Roider, J., and Birngruber, R. (2012). Real-time temperature determination during retinal photocoagulation on patients. *Journal of Biomedical Optics*, 17(6), 061219–1–10.

Herzog, C., Thomsen, O., Schmarbeck, B., Siebert, M., and Brinkmann, R. (2018). Temperature-controlled laser therapy of the retina via robust adaptive $\mathcal{H}_\infty$-control. *Automatisierungstechnik*, 66(12), 1051–1063.

Ljung, L. (1999). *System Identification, Theory for the User*. Prentice-Hall Inc. USA, 2nd edition edition.

Ljung, L. (2018). *System Identification Toolbox^{TM} User's Guide, Matlab 2018b*. The Mathworks, Inc.

Mainster, M. (1999). Decreasing retinal photocoagulation damage: Principles and techniques. *Seminars in Ophthalmology*, 14(4), 200–209.

Schlott, K., Koinzer, S., Ptaszynski, L., Bever, M., Baade, A., Roider, J., Birngruber, R., and Brinkmann, R. (2012). Automatic temperature controlled retinal photocoagulation. *Journal of Biomedical Optics*, 17(6), 061223–1–8.

Skogestad, S. and Postlethwaite, I. (2005). *Multivariable Feedback Control - Analysis and Design*. John Wiley & Sons, Ltd.

Zhou, K. and Doyle, J. (1998). *Essentials of Robust Control*. Prentice-Hall, Upper Saddle River, NJ.